Hindawi
Journal of Chemistry
Volume 2020, Article ID 9619461, 10 pages
https://doi.org/10.1155/2020/9619461

Research Article

Synthesis, Adsorption, and Recognition Properties of a Solid Symmetric Tetramethylcucurbit[6]uril-Based Porous Supramolecular Framework

Fei-Yang Tian, Rui-Xue Cheng, Yun-Qian Zhang, Zhu Tao, and Qian-Jiang Zhu

Key Laboratory of Macrocyclic and Supramolecular Chemistry of Guizhou Province, Guizhou University, Guiyang 550025, China

Correspondence should be addressed to Zhu Tao; gzutao@263.net

Received 17 August 2019; Accepted 4 February 2020; Published 21 March 2020

Academic Editor: Takayuki Ebata

In this work, we reported a porous supramolecular framework (**A**) constructed of a symmetric tetramethylcucurbit[6]uril (TMeQ[6]) in aqueous HCl solutions; the driving force was the outer surface interaction of cucurbit[*n*]urils, as well as hydrogen bonding between latticed water molecules and portal carbonyl oxygens of TMeQ[6]. Adsorption experimental results revealed that the porous supramolecular framework can absorb certain fluorophore guests (**FG**s) to form luminescent assemblies (**FG@A**s) by fluorescence enhancement or colour change, and some of them can respond to certain volatile organic compounds. Thus, the TMeQ[6]-based supramolecular framework could be used as a sensor for certain gas or volatile compounds.

1. Introduction

Symmetric tetramethylcucurbit[6]uril (TMeQ[6]) is the earliest reported partial alkyl-substituted cucurbit[*n*]uril in our laboratory [1]. TMeQ[6] was condensed by using the diether of dimethyl-glycoluril (1) and the dimer of glycoluril (2) in aqueous HCl solutions. The free TMeQ[6] is ellipsoid (Figure 1) due to the tension between the two substituted methyl groups on the dimethyl-glycoluril and has well water solubility. Therefore, TMeQ[6] was used to replace the water insoluble Q[6] when we investigated Q[6]-based host-guest interaction and coordination with metal cations in neutral aqueous solutions. For example, the structure feature of TMeQ[6] was confirmed using the host-guest interaction of TMeQ[6] with 2,2′-bipyridine in neutral aqueous solution when it was first isolated [1]. Then, a series of host-guest interaction studies on TMeQ[6] were reported [2–6]; for example, the interaction of TMeQ[6] with three hydrochloride salts of phenylephrine isomers was investigated using a competitive interaction method which could explain how subtle differences in the structure of the title isomers lead to a significant difference in the stability of the corresponding host-guest inclusion complexes with the TMeQ[6] [2]; using TMeQ[6], binding interactions with a series of alkyldiammonium ions in aqueous solution were investigated in detail [3]; moreover, investigation of the host-guest interaction between TMeQ[6] and 2-(4-methoxyphenyl)-1H-imidazo[4,5-f][1,10]phenanthroline hydrochloride salt (guest 1) revealed that TMeQ[6] can trigger fluorescence emission of this guest 1 by TMeQ[6], which has been developed to achieve a supramolecular probe capable of recognizing La^{3+} and Ce^{3+} through a dramatic decrease in fluorescence intensity [4]. Also the coordination and interaction of TMeQ[6] with a series of metal ions, such as alkali (A^+), alkaline earth (AE^{2+}), and lanthanide metal ions (Ln^{3+}), showed a difference from those of water insoluble Q[6] [5, 6]. In particular, such differences in the interaction between TMeQ[6] and Ln^{3+} could potentially be used for isolating heavier Ln^{3+} from their lighter counterparts in neutral solution, and lighter lanthanide cations from their heavier counterparts in acidic solution.

Besides the Q[*n*]-based host-guest chemistry [7–12] and coordination chemistry [13–16], the positive electropotential outer surface of cucurbit[*n*]uril has attracted great attention, and Q[*n*]-based outer surface interaction chemistry was proposed in recent years [17]. In this emerging chemistry,

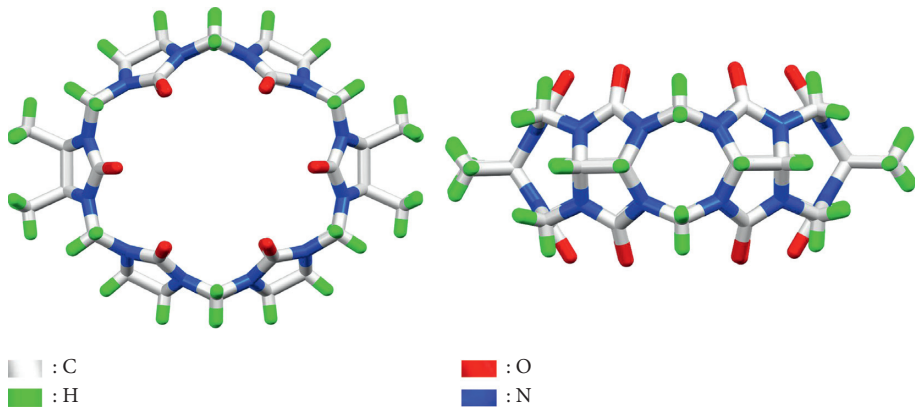

Figure 1: Structure of Symmetric tetramethylcucurbit[6]uril (TMeQ[6], $C_{36}H_{44}O_{12}N_{24}$).

simple Q[*n*]-based supramolecular assembly chemistry based on the outer surface interaction of cucurbit[*n*]uril is becoming an important branch. For example, since 2008, Kim and coworkers have demonstrated a series of simple Q[6]-, Q[7]-, or Q[8]-based supramolecular frameworks [18–21], exhibiting special adsorption for $CH_2{=}CH_2$[19] and CO_2 [20] or showing anisotropic proton conductivity [21]. Nowadays, we know that the outer surface interaction of cucurbit[*n*]urils (Q[*n*]s), which is attributed to the positive electropotential outer surface of Q[*n*]s results in the formation of these novel Q[*n*]-based porous supramolecular frameworks [17]. Our group and others also demonstrated a series of Q[*n*]-based porous supramolecular frameworks in the absence and presence of different structure directing agents in different mediums [14, 22–31]. For example, Thallapally and Tian demonstrated a crystalline form of Q[6] *via* the outer surface interaction of cucurbit[*n*]uril, which exhibited high thermal stability, permanent porosity, and the highest specific surface area of any known solid-state forms of Q[6] [22]. When Lu and coworkers investigated the drug delivery function of Q[7], they obtained a Q[7]-based supramolecular framework through the outer surface interaction of Q[*n*]s [23]. Moreover, Q[6] can arrange into a supramolecular polycatenane stabilised by the outer surface interaction of cucurbit[6]urils [24]. Cao and coworkers demonstrated a series of supramolecular compounds constructed from decamethylcucurbit[5]uril (Me_{10}Q[5]) and different HPAs or POMs; they found that the Me_{10}Q[5]-HPA or POMs-based supramolecular framework exhibited reversible photochromic properties as well as excellent photocatalytic activity toward the degradation of methyl orange and rhodamine B under visible light irradiation [14, 25, 26]. Recently, we demonstrated a series of simple Q[10]-based supramolecular frameworks in the absence and presence of structure directing agents in aqueous HCl or HNO_3 solutions [27–30], which not only exhibited sequence selectivity isolation of specific metal cations, thus leading to these architectures being used as metal-selective materials [28], but also exhibited novel adsorption capacities for certain dyes and became novel luminescent materials [29], which could have special selective response to certain volatile compounds [30]. More recently, Fedin and coworkers demonstrated a series of novel supramolecular frameworks based on Q[6] and mono-/polynuclear bismuth(III)- and mercury(II)-ions. This work further extended the research on the construction of Q[*n*]-based supramolecular frameworks assembled through the inorganic anion as the structure directing agents [31]. Thus, we focused on the simple Q[*n*]-based porous supramolecular frameworks, their adsorption properties for dyes, and their response to various volatile organic compounds. In the present work, the symmetric tetramethylcucurbit[6]uril (TMeQ[6]) was selected as building block, and a facile TMeQ[6]-based porous supramolecular framework was prepared from aqueous HCl (1–3 M) solutions (**A**). This supramolecular framework can absorb various fluorophore guests (**FG**s), resulting in the formation of luminescent assemblies (**FG@A**s) by fluorescence enhancement or colour change. Moreover, most **FG@A** systems exhibited response to certain volatile organic compounds (**VOC**s) and could be used as solid sensors.

2. Experimental Section

2.1. Materials. TMeQ[6] was synthesised by literature method. Other chemicals (analytical grade) were obtained from Aladdin and used without further purification.

2.2. Synthesis of TMeQ[6]-Based Supramolecular Framework (A). Solid TMeQ[6] was dissolved in aqueous HCl solutions (1~3 M), in particular in 2 M aqueous HCl solution with the highest yield and in the shortest period. Colourless crystals **A** with a formula TMeQ[6] $24H_2O$ occurred overnight with about 80% yield.

2.3. Measurements. All ^{1}H NMR spectra, including those for titration experiments, were recorded at 20°C in D_2O on a JEOL JNM-ECZ400s spectrometer.

2.4. X-ray Crystallography. Crystallographic data collections for **A** were carried out on a Bruker Smart Apex II CCD area detector diffractometer with graphite-monochromated Mo Kα radiation ($\lambda = 0.71073$ Å, $\mu = 0.828$ mm^{-1}) using ω-scan

technique and fitted with a nitrogen cold stream (−30°C). The diffraction data were integrated by using the SAINT program, which was also used for the intensity corrections for the Lorentz and polarization effects, and semiempirical absorption corrections were applied using SADABS program. The structure was solved by direct methods, and all of the nonhydrogen atoms were refined anisotropically by the full-matrix least-squares method on F [2] using the SHELXS-97 and SHELXL-97 program packages, respectively [32, 33]. Carbon-bound hydrogen atoms were introduced at calculated positions and were treated as riding atoms with an isotropic displacement parameter equal to 1.2 times that of the parent atom. Twenty-four water molecules in **A** were omitted using the SQUEEZE option of the PLATON program. Analytical expressions for neutral-atom scattering factors were employed, and anomalous dispersion corrections were incorporated. The crystallographic data of **A** have been deposited at the Cambridge Crystallographic Data Centre as supplementary publication no. CCDC-1873879, containing the supplementary crystallographic data for this paper, which can be obtained free of charge from the Cambridge Crystallographic Data centre *via* ww.ccdc.cam.ac.uk/data_request/cif.

2.5. Preparation of Solid-State FG@A Fluorescent Materials. TMeQ[6]-based **A** 1.0 g was added to 4.0 mL 5×10^{-3} M**FG** acetonitrile solution with stirring for 1 h and filtered, and solid materials with different colour fluorescence were collected.

2.6. Adsorption and Response Investigations of FG@A for VOCs. The activated **FG@A** (0.5–1.0 g) was added to a tared open glass phial, and then the phial was put into a vacuum desiccator and evacuated using a vacuum pump until the sample achieved a constant weight. A few mL of the **VOC** (methanol, ethanol, ethyl ether, acetonitrile, acetone, dichloromethane, trichloromethane, tetrachloromethane, and so on) was then added to another open glass phial, put into the same vacuum desiccator, and resealed. The weight change was measured and corresponding solid fluorescence spectra were determined at ~1–60 min intervals over several hours to obtain the vapour adsorption profile.

2.7. Measurement of Fluorescence Spectra of Solid FG@A Assemblies. Fluorescence spectra of solid **FG@A** assemblies before and after adsorbing **VOC**s were recorded at 25°C using a Varian Cary Eclipse spectrofluorometer (Varian, Inc., Palo Alto, CA, USA), respectively.

3. Result and Discussion

3.1. Crystal Structures of Compounds A. Various TMeQ[6]-based supramolecular assemblies or frameworks were formed from TMeQ[6] molecules in the presence of inorganic anions or aromatic compounds through the outer surface interaction of cucurbit[n]urils in the different mediums [5, 6]. Herein, a simple TMeQ[6]-based supramolecular framework was generated from aqueous HCl (1~3 M) solutions (**A**). Above or below this acidity range, not only is the yield of TMeQ[6] crystals low, but also it takes too long. In aqueous HCl (2 M) solution, TMeQ[6] crystals occur in 3 h, left overnight, and the yield reaches up to about 80%. In this TMeQ[6]-based supramolecular assembly, each TMeQ[6] molecule (the central TMeQ[6]) interacts with four neighbouring TMeQ[6] molecules through the so-called outer surface interaction of cucurbit[n]uril (Figure 2(a)) [17]. The portal carbonyls of the central TMeQ[6] are always close to the outer surface without substituted methyl groups of two neighbouring TMeQ[6] molecules; in turn, portal carbonyls of another two neighbouring TMeQ[6] molecules are always close to the outer surface without substituted methyl groups of the central TMeQ[6] molecule, owing to the positive electropotential outer surface of cucurbit[n]urils. Thus, further extension of TMeQ[6] molecules results in the formation of a TMeQ[6]-based 2D supramolecular framework, in which every four TMeQ[6] molecules can arrange into two different square pores with sections of ~25 and ~62 Å^2, respectively (Figure 2(b)). A close inspection revealed that the detailed interactions mainly include dipole interaction between portal carbonyl oxygens of a TMeQ[6] molecule and positive electropotential methane (O4-H35, O3-H34, O2-H34; O8-H15, O9-H15, O10-H14), methylene (O4-H37B, O2-H31A; O8-H17A, O10-H11A, O11-H12A), and even methyl groups (O4-H39C; O8-H19C) on the outer surface of a neighbouring TMeQ[6] molecule (Figures 2(c) and 2(d)), in addition to the hydrogen bonding between the latticed water molecules and portal carbonyl oxygens of neighbouring TMeQ[6] molecules in **A** (omitted for clarity). The distances between portal carbonyl oxygens of TMeQ[6] molecules and methine, and methylene and methyl protons from neighbouring TMeQ[6] molecules are in the range 2.343~2.717 Å. Figure 2(e) shows the TMeQ[6]-based supramolecular framework stacked by the TMeQ[6]-based 2D supramolecular frameworks with ~3 Å gaps; Figure S1 shows the TMeQ[6]-based supramolecular framework with numerous channels with sections of about 90 Å^2 in compound **A**. All channels in **A** are filled with large amount of water molecules (the latticed water molecules), which link TMeQ[6] molecules through hydrogen bonding with portal carbonyl oxygens of TMeQ[6] molecules in **A**. Single crystal X-ray diffraction analysis reveals that TMeQ[6]-based porous supramolecular assembly has the characteristics of frameworks and belongs to a typical supramolecular organic framework (SOF). Therefore, the TMeQ[6]-based supramolecular framework could find applications in catalysis, sensors, adsorption, ion exchange processes, and so on. Herein, we first considered the adsorption properties in the present work.

Powder X-ray diffraction spectrum of the bulk of **A** essentially consists of that of simulation of pure crystalline phases (Figure S2 in the ESI). Analysis of the thermal stabilities of **A** includes differential scanning calorimetry (DSC) and thermogravimetry (TG) (Figure S3 in the ESI). For the air-dried **A**, the DSC with TG curves suggested that water molecules of crystallization were first eliminated with weight losses of ~28% (calcd. 25%) when the temperature was increased from ambient to about 200°C. Further weight loss was observed starting from about 300°C, and sharp weight

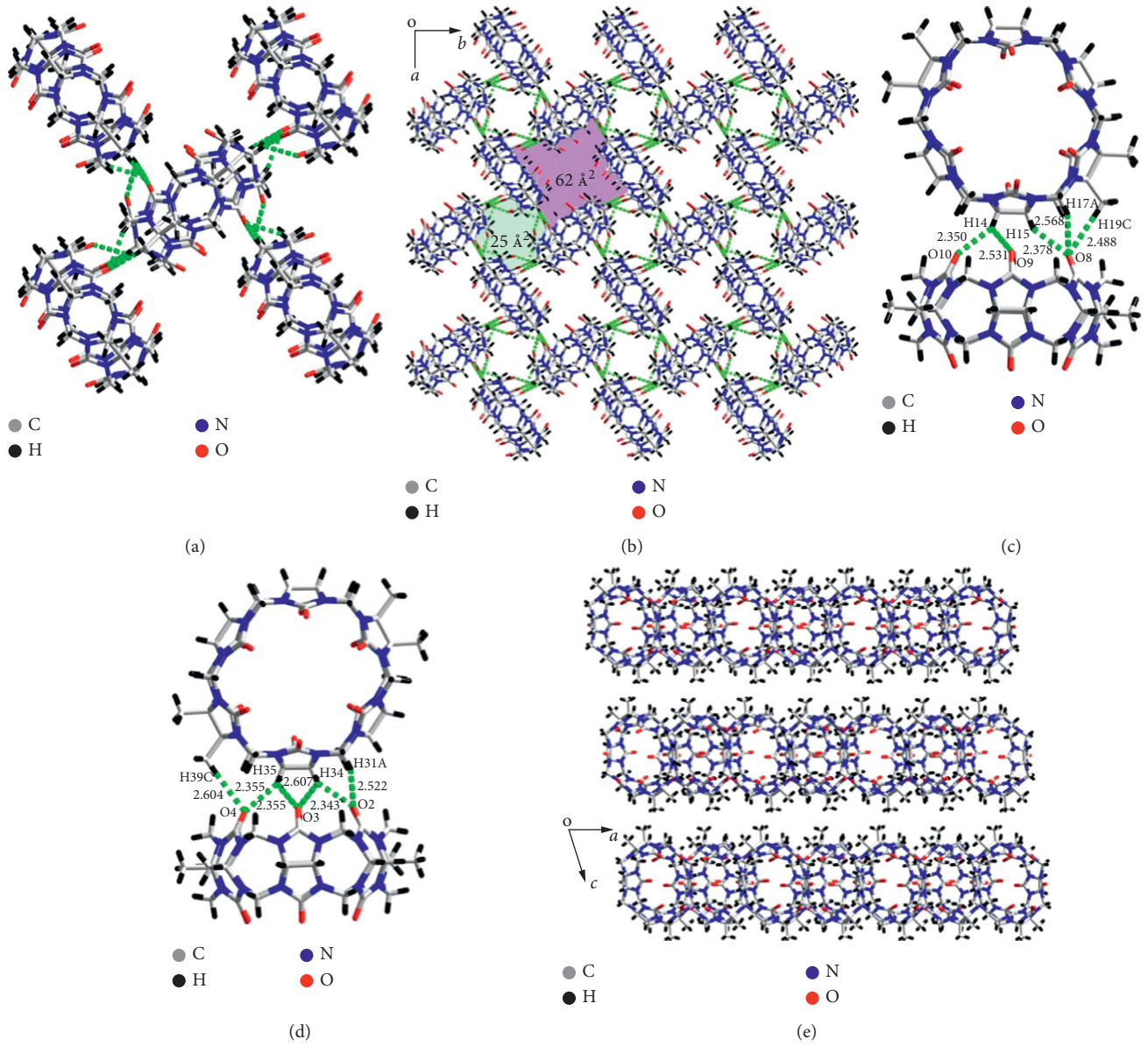

Figure 2: Crystal structure of (a) supramolecular interactions between the central TMeQ[6] molecule and four neighbouring TMeQ[6] molecules in **A**; (b) a TMeQ[6]-based 2D supramolecular assembly; (c, d) detailed interactions between neighbouring TMeQ[6] molecules and crystals; (e) stacking structure from *ac* plane in compound **A**.

losses were incurred at about 400°C, suggesting the decomposition of TMeQ[6].

3.2. Adsorption Properties of TMeQ[6]-Based Porous Supramolecular Framework. Quite a few experimental results have proven that Q[*n*]-based porous supramolecular frameworks can take up various dyes and fused ring compounds and form solid fluorescent assemblies [29, 30]. In the present case, different pores, gaps, spaces, and channels can be observed in the TMeQ[6]-based porous supramolecular assembly (**A**). Loading of porous assembly **A** was tested with 15 fluorophore guests (**FG**s): 4,4′-dihydroxybenzophenone (**FG**1), levofloxacin (**FG**2), 1-pyrenecarboxaldehyde (**FG**3), rhodamine B (**FG**4), 7-hydroxycoumarin (**FG**5), 1,10-phenanthroline (**FG**6), levofloxacin Astrazon Pink FG (**FG**7), 1-pyrenemethylamine hydrochloride (**FG**8), neocuproine hydrochloride (**FG**9), pyrene (**FG**10), 8-hydroxyquinoline (**FG**11), 1-naphthol (**FG**12), dansyl chloride (**FG**13),2-(3*H*-[1,2,3]triazolo[4,5-*b*]pyridine-3-yl)-1,1,3,3-tetramethylisouronium (**FG**14), and 2-(4-(dimethylamino) phenyl)-3,6-dimethylbenzo[*d*]thiazol-3-ium (**FG**15). Most of the products (**FG@A**s) displayed enhanced fluorescence emission and/or altered fluorescence colour, with the exception of rhodamine B (**FG**4) and levofloxacin Astrazon Pink FG (**FG**7) which resulted in weak fluorescence of **FG**4@**A** and **FG**7@**A**. A comparison of the fluorescence spectra of guest **FG**x ($x = 1–15$) and the corresponding luminescent material **FG**x@**A** is shown in the figures in the second column in Table S1. For example, loading **A** with **FG**6 by

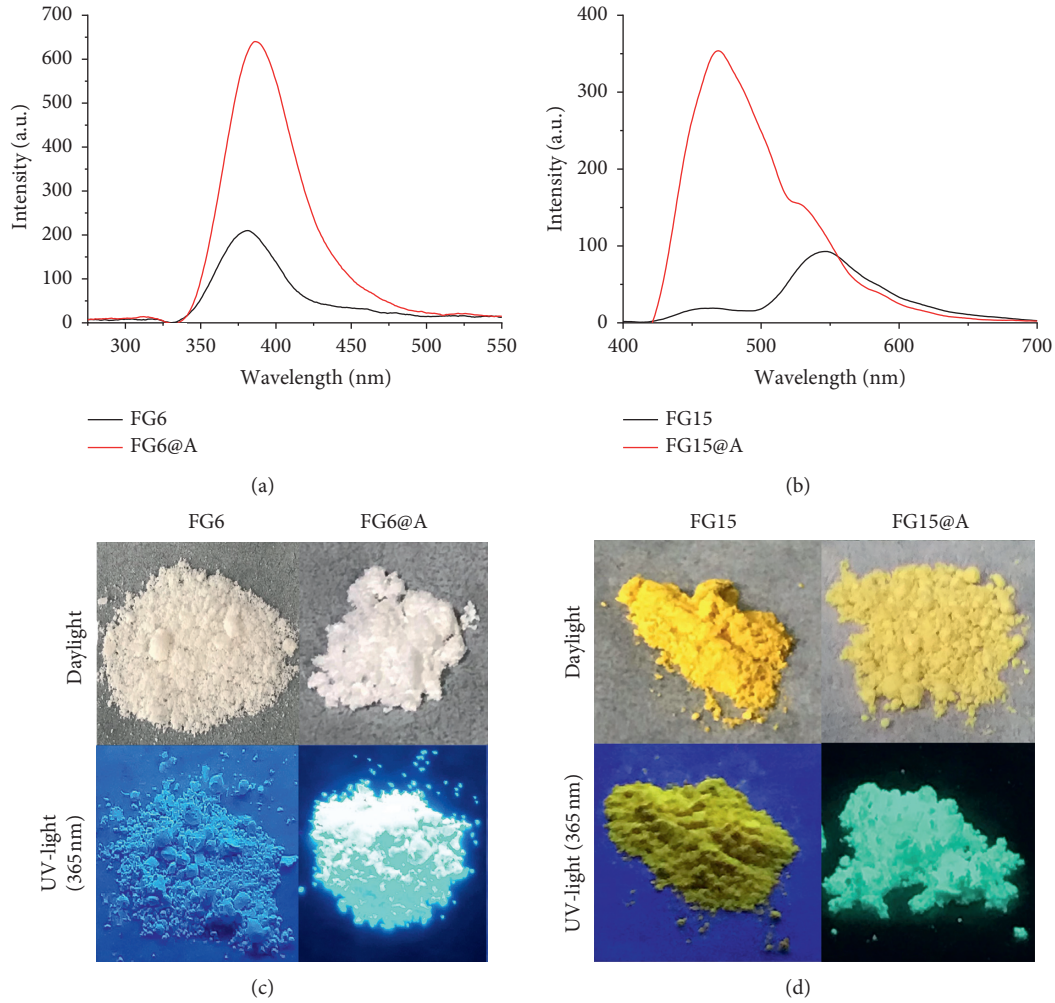

Figure 3: Comparison of fluorescence spectra of (a) **FG**6 and solid **FG**6@**A**; (b) **FG**15 and solid **FG**15@**A**; the colour of (c) **FG**6 and solid **FG**6@**A**; (d) **FG**15 and solid **FG**15@**A** under daylight and UV light (365 nm).

immersing **A** in an acetonitrile solution containing **FG**6 yielded luminescent material **FG**6@**A** that exhibited a ~2.5-fold increase in fluorescence enhancement compared with the free **FG**6 (Figure 3(a)). Meanwhile, loading **A** with **FG**15 yielded luminescent material **FG**15@**A** that exhibited not only a ~2.5-fold increase in fluorescence enhancement but also a fluorescence colour change from green to blue compared with the free **FG**15 (Figure 3(b)). The amount of **FG**6, **FG**15, or other adsorbates extracted by TMeQ[6]-based assembly **A** from the acetonitrile solution could be measured using ^{1}H NMR to compare the integrity before and after extracting the adsorbates (Figure S5 and Table S2). In general, loading porous framework **A** with a fluorescent guest could change conformation or aggregation state of the fluorescent guest and result in its fluorescence enhancement or quenching.

Recent studies have shown that Q[*n*]-based supramolecular assemblies or frameworks can adsorb a variety of **VOC**s, whereas the adsorbed **VOC** could influence the florescence properties of the resulting **FG**@**A** luminescent materials [29,30]. Thus, the adsorption of 12 common **VOC**s was tested: dichloromethane, trichloromethane, tetrachloromethane, methanol, ethanol, acetone, acetonitrile, ethyl ether, benzene, toluene, formaldehyde, and tetrahydrofuran. The results revealed that the **FG**@**A** systems exhibited different responses to the selected **VOC**s, via fluorescence quenching or enhancement (Figures S5–S17). For example, **FG**10@**A** exhibited little or no response to most **VOC**s, except alcohols, acetone, and acetonitrile, as demonstrated by significant fluorescence enhancement (Figure 4(a)). **FG**2@**A** and **FG**11@**A** exhibited similar responses to these via a significant fluorescence enhancement. Meanwhile, most **FG**@**A** systems exhibited little or no responses to all selected **VOC**s (Figures S5, S7–S9, S15, and S16). Because the free **FG**4 and **FG**7 and the corresponding **FG**4@**A** and **FG**7@**A** systems all showed weak fluorescence, the adsorption properties of the selected **VOC**s were not investigated in the present work. It is interesting that **FG**15@**A** exhibited little or no response to most **VOC**s, whereas loading **FG**15@**A** with trichloromethane resulted in obvious fluorescence enhancement, suggesting that **FG**15@**A** possessed high selectivity for trichloromethane (Figure 4(b)).

More detailed investigations on these systems were performed by assessing fluorescence changes *via* real-time

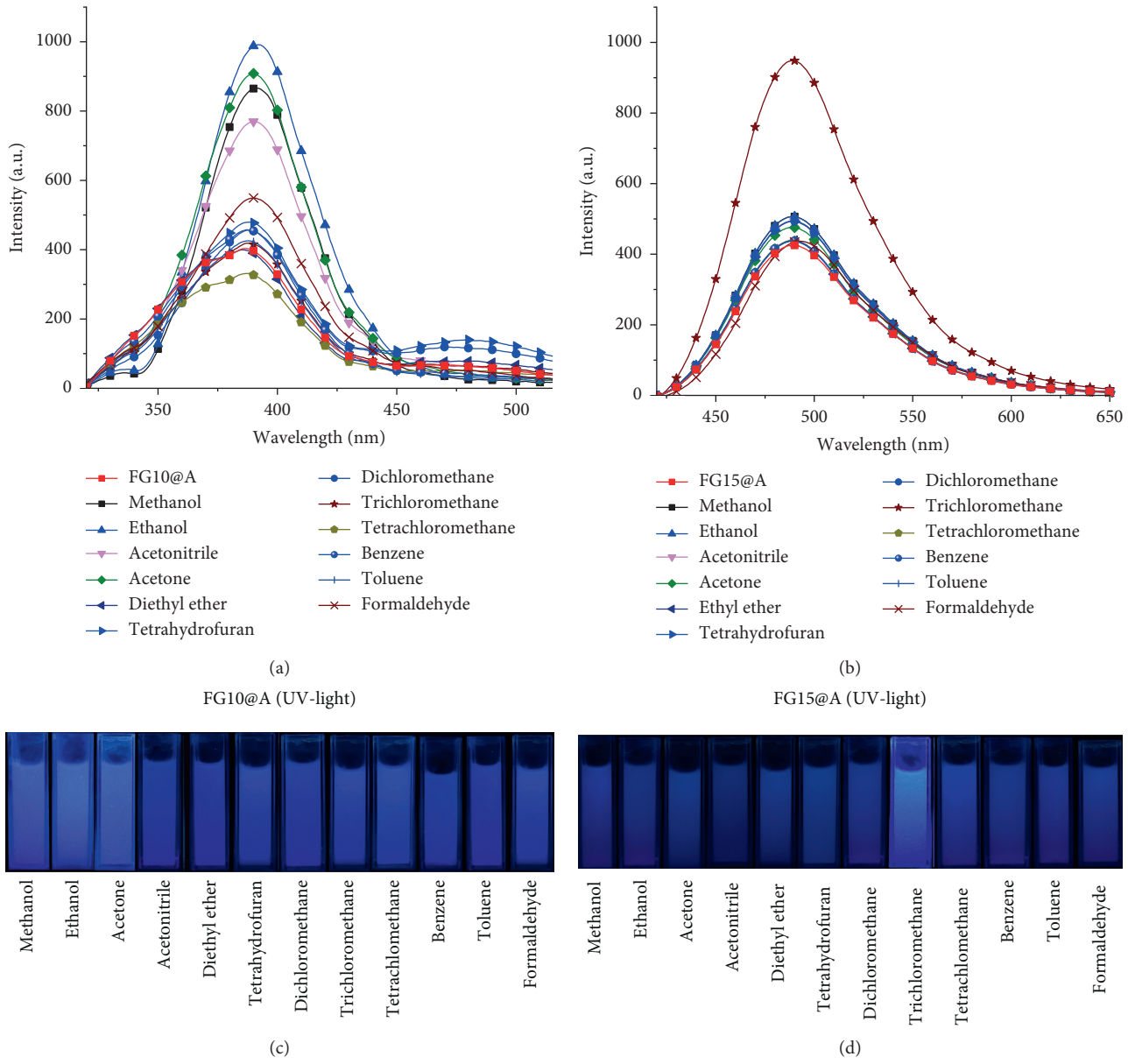

Figure 4: Fluorescence spectra of (a) **FG**10@**A**; (b) **FG**15@**A** loaded with the 12 **VOC**s, respectively; (c, d) the corresponding photographs of **FG**10@**A** and **FG**15@**A** containing selected **VOC**s under UV light (365 nm).

monitoring of the uptake of the selected **VOC**s. For example, titration fluorescence spectra of the loading of **FG**10@**A** with ethanol revealed a rapid increase in fluorescence intensity with increasing the adsorption time or the amount of absorbed formaldehyde (Figure 5(a)). Figure 5(b) shows that the fluorescence intensity of solid **FG**10@**A** at 392 nm increased with increasing the adsorption time; it took about 20 min to reach the max value (the equilibration time). Figure 5(c) shows the adsorption profile, and the adsorption or saturation adsorption of **FG**10@**A** for ethanol increased by 4% (wt%) within about 6 h. The equilibration time (20 min) was obviously much shorter than the saturation adsorption time (6 h). The response of a **FG**/**A** luminescent material to **VOC** was dependent on the properties of **FG** and **VOC**, and the detection limit (DL) of the **FG**/**A** luminescent material for **VOC**s varied with the different luminescent materials and the different **VOC**s. Based on the intensity/time curve data (Figure 5(b)) and the adsorption/time data (Figure 5(c)) used in the interpolation method, ΔI *vs*. the amount of ethanol adsorbed on solid **FG**10@**A** was plotted (Figure 5(d)), and DL was calculated by multiplying the standard derivation of ten measurements in the absence of ethanol by three, and dividing by the slope of the linear calibration curve over a low concentration range. The DL of solid **FG**10@**A** for ethanol was $\sim 7.23 \times 10^{-7}$ mol·gram^{-1}. Titration experiments of the loading of **FG**10@**A** with acetone were also performed (Figures S18). The DL of solid **FG**10@**A** with acetone was 3.71×10^{-7} mol·gram^{-1}. The titration fluorescence spectra of the loading of solid **FG**15@**A** with trichloromethane also showed a rapid fluorescence

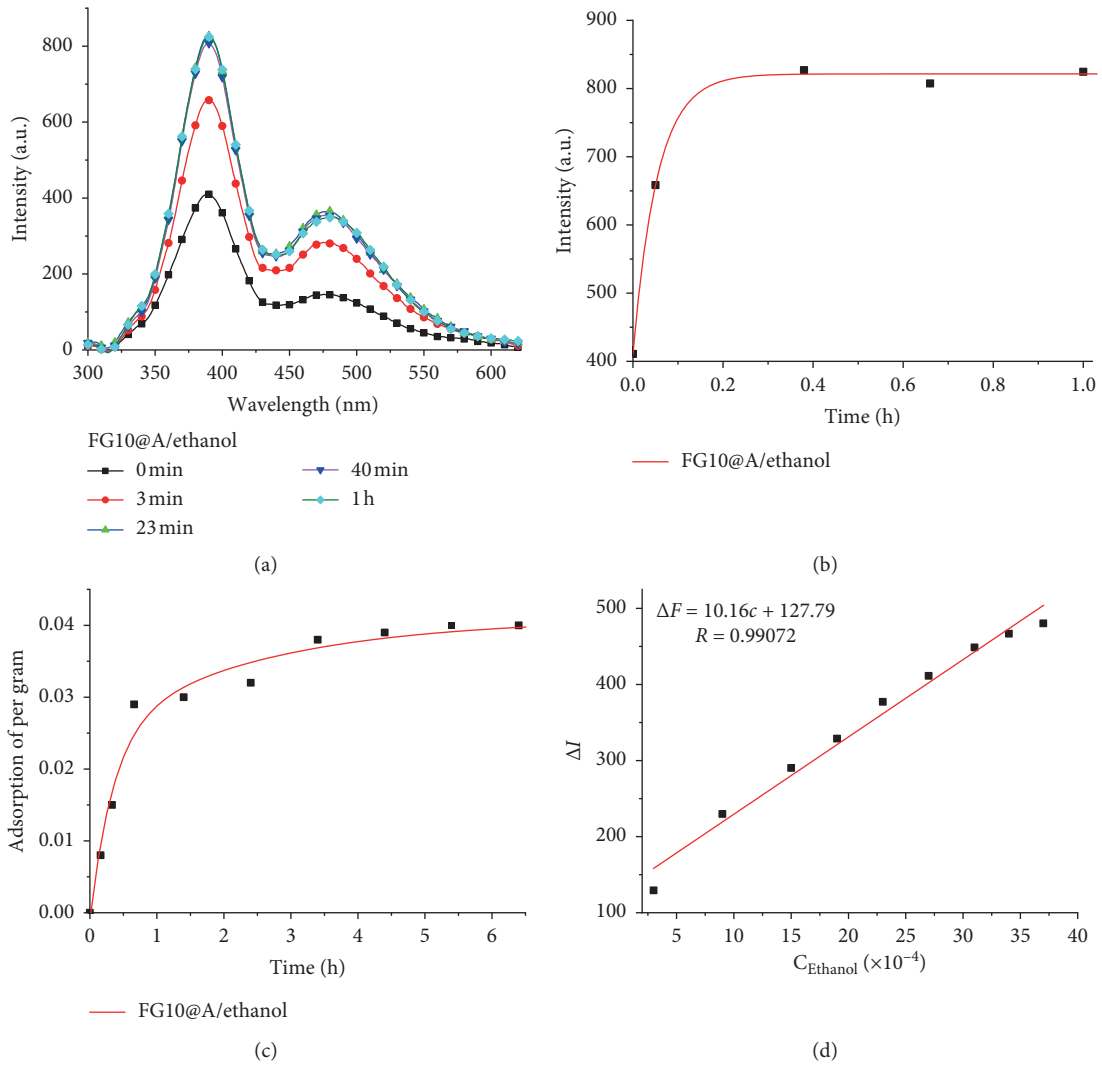

Figure 5: (a) Titration fluorescence spectra of the loading of **FG**10@**A** with ethanol; (b) change in fluorescence intensity of **FG**10@**A** with increasing adsorption time; (c) adsorption profile of the loading of ethanol in **FG**10@**A**; (d) plot of ΔI *vs.* the amount of ethanol adsorbed by solid **FG**10@**A**.

enhancement with increasing adsorption time (Figure 6(a)). Figure 6(b) shows the change in fluorescence intensity of solid **FG**15@**A** with increasing adsorption time at 470 nm; it reached the maximum after 0.5 h. Figure 6(c) shows the adsorption profile of trichloromethane loading with **FG**15@**A**, and the adsorption capacity increased by ~40% (wt%) within 2 h. Based on the data in Figures 6(b) and 6(c), ΔI *vs.* the amount of trichloromethane adsorbed by solid **FG**15@**A** was plotted (Figure 6(d)), and the DL of solid **FG**15@**A** for trichloromethane was determined to be 2.76×10^{-8} mol·gram^{-1}.

In the present work, there are some other **FG**@TMeQ[6]-based luminescent assemblies which exhibit distinct selective response to certain volatile compounds, including the following: **FG**2@**A** to ethanol and dichloromethane; **FG**11@**A** to ethanol, dichloromethane, and benzene. The detailed adsorption properties of these systems have also been examined, and the detailed experimental results are shown in Figures S19–S23. The DLs of solid **FG**2@**A** for ethanol and dichloromethane were determined to be 9.59×10^{-8} and 3.71×10^{-7} mol·gram^{-1}, respectively, and the DLs of solid **FG**11@**A** for ethanol, dichloromethane, and benzene were determined to be 6.36×10^{-8}, 3.87×10^{-7}, and 4.39×10^{-7} mol·gram^{-1}, respectively. In general, a change in fluorescence emission of an **FG** molecule could be influenced by changes in molecular configuration or aggregation state; loading of the **FG** into a porous assembly such as the Q[*n*]-based porous supramolecular assemblies could alter its configuration or aggregation state, resulting in fluorescence enhancement or quenching of the **FG**. Thus, we loaded the simple TMeQ[6]-based porous supramolecular assemblies with common fluorescent guests to yield novel luminescent materials. Moreover, most of the resulting solid **FG**@**A** systems responded to common **VOC**s, suggesting that the adsorbed **VOC**s influence the molecular structure configuration and aggregation state or charge distribution of the loaded **FG** molecule through intermolecular interactions between the loaded **FG**, the adsorbed **VOC**, and TMeQ[6]

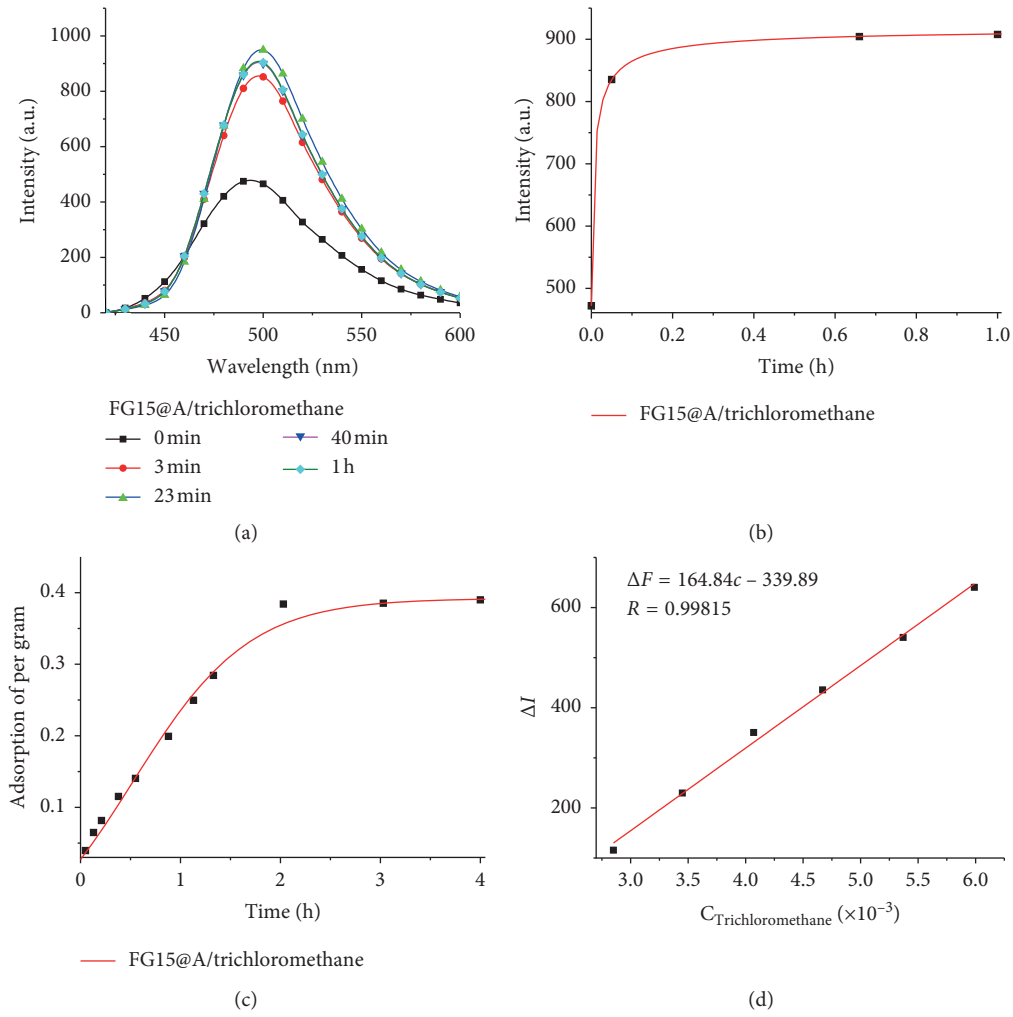

Figure 6: (a) Titration fluorescence spectra of the loading of **FG**15@**A** with trichloromethane; (b) change in fluorescence intensity of **FG**15@**A** with increasing adsorption time; (c) adsorption profile of the loading of trichloromethane by solid **FG**15@**A**; (d) plot of ΔI *vs.* the amount of trichloromethane adsorbed by solid **FG**15@**A**.

molecules in the framework. Generally, when the adsorbed **VOC**s were removed, the fluorescence of solid **FG@A** was recovered. Analysis of the lifetime of the adsorption capacity or fluorescence emission revealed that some **FG@A-VOC** systems exhibited reversible adsorption and were relatively stable (Figures S24 and S25). Previous studies have proven that the adsorption of neat **FG** for **VOC** was unable to induce an obvious fluorescence change in the selected **FG**s. Similar phenomena can be observed in the present work (Figure S26).

4. Conclusion

In summary, we prepared a porous supramolecular framework (**A**) by simple crystallization TMeQ[6] in aqueous HCl solutions (1–3 M). Crystal structure analysis showed that the framework contained two different square holes in each TMeQ[6]-based layer and numerous gaps between the layers. The driving force was derived from the outer surface interaction of cucurbit[*n*]urils, as well as hydrogen bonding networks among the latticed water molecules with electrostatic potential negative portal carbonyl groups of TMeQ[6]. The TMeQ[6]-based porous supramolecular framework (**A**) exhibited special adsorption for certain fluorophore guests to form solid fluorescent materials (**FG**/**A**s) with certain fluorescence emission, which can further adsorb different common volatile organic compounds (**VOC**s), accompanied by fluorescence response (enhancement or quenching). Thus, preparing porous Q[*n*]-based supramolecular frameworks, loading TMeQ[6]-based porous supramolecular assemblies with **FG**s yielded solid fluorescent sensors, and detecting **FG**/**A**s response to certain **VOC**s could launch a new field of Q[*n*]-based supramolecular chemistry. More extensive investigations of these Q[*n*]-based supramolecular assemblies and their functions are currently underway.

Data Availability

The PXRD, NMR, and fluorescence spectra and adsorption data used to support the findings of this study are included within the supplementary information file.

Conflicts of Interest

The authors declare that they have no conflicts of interest.

Acknowledgments

The authors thank the National Natural Science Foundation of China (Grant nos. 51663005, 21761007, and 21871064) and Science and Technology Plan Project of Guizhou Province (nos. 20175788 and 20185781) for supporting this work.

Supplementary Materials

Fig. S1: stacking structure from ab plane in compound A. Fig. S2: powder X-ray diffraction analyses of A (top) and comparison with simulation (bottom). Fig. S3: TG (top) and DTA (bottom) curves of A in N2. Table S1: first column: selected 15 fluorophore guests (FGs); second column: general survey of loading A with 15 fluorophore guests (FGs) to form luminescent assemblies (FG@As) by comparison of colour and fluorescence spectra of FG and solid FG@As, respectively. Fig. S4: ^{1}H NMR spectra in deuterated acetonitrile: (a) 0.5 mL 0.01 M FG2 added to 10 mg A; (b) 0.5 mL 0.01 M FG2; (c) 0.5 mL 0.01 M FG5 added to 10 mg A; (d) 0.5 mL 0.01 M FG5; (e) 0.5 mL 0.01 M FG10 added to 10 mg A; (f) 0.5 mL 0.01 M FG10; (g) 0.5 mL 0.01 M FG11 added to 10 mg A; (h) 0.5 mL 0.01 M FG11; (i) 0.5 mL 0.01 M FG15 added to 10 mg A; (j) 0.5 mL 0.01 M FG15. Table S2: normalised adsorption data of A for five dyes, respectively (mol/g). Fig. S5: general survey of fluorescence spectra of FG1@A loaded with the 12 VOCs, respectively. Fig. S6: general survey of fluorescence spectra of FG2@A loaded with the 12 VOCs, respectively. Fig. S7: general survey of fluorescence spectra of FG3@A loaded with the 12 VOCs, respectively. Fig. S8: general survey of fluorescence spectra of FG5@A loaded with the 12 VOCs, respectively. Fig. S9: general survey of fluorescence spectra of FG6@A loaded with the 12 VOCs, respectively. Fig. S10: general survey of fluorescence spectra of FG8@A loaded with the 12 VOCs, respectively. Fig. S11: general survey of fluorescence spectra of FG9@A loaded with the 12 VOCs, respectively. Fig. S12: general survey of fluorescence spectra of FG10@A loaded with the 12 VOCs, respectively. Fig. S13: general survey of fluorescence spectra of FG11@A loaded with the 12 VOCs, respectively. Fig. S14: general survey of fluorescence spectra of FG12@A loaded with the 12 VOCs, respectively. Fig. S15: general survey of fluorescence spectra of FG13@A loaded with the 12 VOCs, respectively. Fig. S16: general survey of fluorescence spectra of FG14@A loaded with the 12 VOCs, respectively. Fig. S17: general survey of fluorescence spectra of FG15@A loaded with the 12 VOCs, respectively. Fig. S18: (a) titration fluorescence spectra of the loading of FG10@A with acetone; (b) change in fluorescence intensity of FG10@A with increasing adsorption time; (c) adsorption profile of the loading of acetone in FG10@A; (d) plot of ΔI vs. the amount of acetone adsorbed by solid FG10@A. Fig. S19: (a) titration fluorescence spectra of the loading of FG2@A with ethanol; (b) change in fluorescence intensity of FG2@A with increasing adsorption time; (c) adsorption profile of the loading of ethanol in FG2@A; (d) plot of ΔI vs. the amount of ethanol adsorbed by solid FG2@A. Fig. S20: (a) titration fluorescence spectra of the loading of FG2@A with dichloromethane; (b) change in fluorescence intensity of FG2@A with increasing adsorption time; (c) adsorption profile of the loading of dichloromethane in FG2@A; (d) plot of ΔI vs. the amount of dichloromethane adsorbed by solid FG2@A. Fig. S21: (a) titration fluorescence spectra of the loading of FG11@A with ethanol; (b) change in fluorescence intensity of FG11@A with increasing adsorption time; (c) adsorption profile of the loading of ethanol in FG11@A; (d) plot of I vs. the amount of ethanol adsorbed by solid FG11@A. Fig. S22: (a) titration fluorescence spectra of the loading of FG11@A with dichloromethane; (b) change in fluorescence intensity of FG11@A with increasing adsorption time; (c) adsorption profile of the loading of dichloromethane in FG11@A; (d) plot of ΔI vs. the amount of dichloromethane adsorbed by solid FG11@A. Fig. S23: (a) titration fluorescence spectra of the loading of FG11@A with benzol; (b) change in fluorescence intensity of FG11@A with increasing adsorption time; (c) adsorption profile of the loading of benzol in FG11@A; (d) plot of ΔI vs. the amount of benzol adsorbed by solid FG11@A. Fig. S24: lifetime experiments of fluorescence strength of solid FG@As for selected volatile compounds. Fig. S25: lifetime experiments of adsorption capacities of selected solid FG@As for selected VOCs. Fig. S26: the adsorption of neat FG for VOCs. Table S1: first column: selected 15 fluorophore guests (FGs); second column: general survey of loading A with 15 fluorophore guests (FGs) to form luminescent assemblies (FG@As) by comparison of colour and fluorescence spectra of FG and solid FG@As, respectively. (*Supplementary Materials*)

References

[1] Y. Zhao, Y. Q. Shen, S. F. Xue et al., "Synthesis of a symmetrical tetrasubstituted cucurbit[6]uril and its host-guest inclusion complex with 2,2′-bipyridine," *Chinese Science Bulletin*, vol. 49, no. 11, pp. 1111–1116, 2004.

[2] H. Cong, L.-L. Tao, Y.-H. Yu et al., "Interaction between tetramethylcucurbit[6]uril and some pyridine derivates," *The Journal of Physical Chemistry A*, vol. 111, no. 14, pp. 2715–2721, 2007.

[3] B. Yang, L.-M. Zheng, Z.-Z. Gao et al., "Extended and contorted conformations of alkanediammonium ions in symmetrical α, α′, δ, δ′-tetramethylcucurbit[6]uril cavity," *The Journal of Organic Chemistry*, vol. 79, no. 22, pp. 11194–11198, 2014.

[4] Y.-H. Huang, Q.-X. Geng, X.-Y. Jin et al., "Tetramethylcucurbit[6]uril-triggered fluorescence emission and its application for recognition of rare earth cations," *Sensors and Actuators B: Chemical*, vol. 243, pp. 1102–1108, 2017.

[5] W.-J. Chen, D.-H. Yu, X. Xiao et al., "Difference of coordination between alkali- and alkaline-earth-metal ions to a symmetrical α, α′, δ, δ′-tetramethylcucurbit[6]uril," *Inorganic Chemistry*, vol. 50, no. 15, pp. 6956–6964, 2011.

[6] B. Yang, Z.-Z. Gao, J.-H. Lu et al., "Interaction of a symmetrical α, α′, δ, δ′-tetramethyl-cucurbit[6]uril with Ln^{3+}: potential applications for isolation of lanthanides," *CrystEngComm*, vol. 18, no. 26, pp. 5028–5035, 2016.

[7] K. Kim, "Mechanically interlocked molecules incorporating cucurbituril and their supramolecular assemblies," *Chemical Society Reviews*, vol. 31, no. 2, pp. 96–107, 2002.

[8] R. N. Dsouza, U. Pischel, and W. M. Nau, "Fluorescent dyes and their supramolecular host/guest complexes with macrocycles in aqueous solution," *Chemical Reviews*, vol. 111, no. 12, pp. 7941–7980, 2011.

[9] J. Tian, L. Chen, D.-W. Zhang, Y. Liu, and Z.-T. Li, "Supramolecular organic frameworks: engineering periodicity in water through host-guest chemistry," *Chemical Communications*, vol. 52, no. 38, pp. 6351–6362, 2016.

[10] J. Liu, Y. Lan, Z. Yu et al., "Cucurbit[n]uril-based microcapsules self-assembled within microfluidic droplets: a versatile approach for supramolecular architectures and materials," *Accounts of Chemical Research*, vol. 50, no. 2, pp. 208–217, 2017.

[11] W. Liu, S. K. Samanta, B. D. Smith, and L. Isaacs, "Synthetic mimics of biotin/(strept)avidin," *Chemical Society Reviews*, vol. 46, no. 9, pp. 2391–2403, 2017.

[12] J. Murray, K. Kim, T. Ogoshi, W. Yao, and B. C. Gibb, "The aqueous supramolecular chemistry of cucurbit[*n*]urils, pillar[*n*]arenes and deep-cavity cavitands," *Chemical Society Reviews*, vol. 46, no. 9, pp. 2479–2496, 2017.

[13] O. A. Gerasko, M. N. Sokolov, and V. P. Fedin, "Mono- and polynuclear aqua complexes and cucurbit[6]uril: versatile building blocks for supramolecular chemistry pure," *Pure and Applied Chemistry*, vol. 76, no. 9, pp. 1633–1646, 2014.

[14] J. Lü, J.-X. Lin, M.-N. Cao, and R. Cao, "Cucurbituril: a promising organic building block for the design of coordination compounds and beyond," *Coordination Chemistry Reviews*, vol. 257, no. 7-8, pp. 1334–1356, 2013.

[15] X.-L. Ni, X. Xiao, H. Cong et al., "Cucurbit[*n*]uril-based coordination chemistry: from simple coordination complexes to novel poly-dimensional coordination polymers," *Chemical Society Reviews*, vol. 42, no. 24, pp. 9480–9508, 2013.

[16] X.-L. Ni, S.-F. Xue, Z. Tao, Q.-J. Zhu, L. F. Lindoy, and G. Wei, "Advances in the lanthanide metallosupramolecular chemistry of the cucurbit[*n*]urils," *Coordination Chemistry Reviews*, vol. 287, pp. 89–113, 2015.

[17] X.-L. Ni, X. Xiao, H. Cong, Q.-J. Zhu, S.-F. Xue, and Z. Tao, "Self-assemblies based on the "Outer-Surface interactions" of cucurbit[n]urils: new opportunities for supramolecular architectures and materials," *Accounts of Chemical Research*, vol. 47, no. 4, pp. 1386–1395, 2014.

[18] I. Hwang, W. S. Jeon, H.-J. Kim et al., "Cucurbit[7]uril: a simple macrocyclic, pH-triggered hydrogelator exhibiting guest-induced stimuli-responsive behavior," *Angewandte Chemie International Edition*, vol. 46, no. 1-2, pp. 210–213, 2007.

[19] S. Lim, H. Kim, N. Selvapalam et al., "Cucurbit[6]uril: organic molecular porous material with permanent porosity, exceptional stability, and acetylene sorption properties," *Angewandte Chemie International Edition*, vol. 47, no. 18, pp. 3352–3355, 2008.

[20] H. Kim, Y. Kim, M. Yoon et al., "Highly selective carbon dioxide sorption in an organic molecular porous material," *Journal of the American Chemical Society*, vol. 132, no. 35, pp. 12200–12202, 2010.

[21] M. Yoon, K. Suh, H. Kim, Y. Kim, N. Selvapalam, and K. Kim, "High and highly anisotropic proton conductivity in organic molecular porous materials," *Angewandte Chemie International Edition*, vol. 50, no. 34, pp. 7870–7873, 2011.

[22] J. Tian, J. Liu, J. Liu, and P. K. Thallapally, "Identification of solid-state forms of cucurbit[6]uril for carbon dioxide capture," *CrystEngComm*, vol. 15, no. 8, pp. 1528–1531, 2013.

[23] W.-J. Ma, J.-M. Chen, L. Jiang, J. Yao, and T.-B. Lu, "The delivery of triamterene by cucurbit[7]uril: synthesis, structures and pharmacokinetics study," *Molecular Pharmaceutics*, vol. 10, no. 12, pp. 4698–4705, 2013.

[24] X. Cui, W. Zhao, K. Chen, X.-L. Ni, Y.-Q. Zhang, and Z. Tao, "Outer surface interactions of cucurbit[6]uril that trigger the assembly of supramolecular three-dimensional polycatenanes," *Chemistry—A European Journal*, vol. 23, no. 12, pp. 2759–2763, 2017.

[25] J.-X. Lin, J. Lü, R. Cao, J.-T. Chen, and C.-Y. Su, "Supramolecular assembly from decavanadate anion and decamethylcucurbit[5]uril," *Dalton Transactions*, vol. 7, no. 7, pp. 1101–1103, 2009.

[26] J. Lü, J.-X. Lin, X.-L. Zhao, and R. Cao, "Photochromic hybrid materials of cucurbituril and polyoxometalates as photocatalysts under visible light," *Chemical Communications*, vol. 48, no. 5, pp. 669–671, 2012.

[27] Y.-Q. Yao, Q. Liu, Y. Huang et al., "Supramolecular assemblies of cucurbit[10]uril based on outer surface interactions," *Australian Journal of Chemistry*, vol. 70, no. 5, pp. 637–641, 2017.

[28] Y.-Q. Yao, Y.-J. Zhang, C. Huang et al., "Cucurbit[10]uril-based smart supramolecular organic frameworks in selective isolation of metal cations," *Chemistry of Materials*, vol. 29, no. 13, pp. 5468–5472, 2017.

[29] Y.-Q. Yao, Y.-J. Zhang, Y.-Q. Zhang, Z. Tao, X.-L. Ni, and G. Wei, "Multiple efficient fluorescence emission from cucurbit[10]uril-[Cd4Cl16]8--based pillared diamond porous supramolecular frameworks," *ACS Applied Materials & Interfaces*, vol. 9, no. 46, pp. 40760–40765, 2017.

[30] M. Liu, J. Kan, Y. Yao et al., "Multiple efficient fluorescence emission from cucurbit[10]uril-based porous supramolecular frameworks and their recognition properties," *Sensors and Actuators B: Chemical*, vol. 283, pp. 290–297, 2019.

[31] E. Kovalenko, I. Andrienko, D. Samsonenko, and V. Fedin, "Syntheses, crystal structures and physico-chemical properties of supramolecular assemblies based on cucurbit[6]uril and mono- and polynuclear bismuth(III) and mercury(II) halides," *Journal of Molecular Structure*, vol. 1193, pp. 357–364, 2019.

[32] G. M. Sheldrick, "A short history of SHELX," *Acta Crystallographica Section A Foundations of Crystallography*, vol. 64, no. 1, pp. 112–122, 2008.

[33] G. M. Sheldrick, *Shelxl-97 Program for the Solution and Refinement of Crystal Structures*, University of Goettingen, Göttingen, Germany, 1997.